CORE
Metadata, citation and similar papers at core.ac.uk
Provided by Institutional Research Information System University of Turin

Article

Cell Metabolism

Macrophage Metabolism Controls Tumor Blood Vessel Morphogenesis and Metastasis

Graphical Abstract

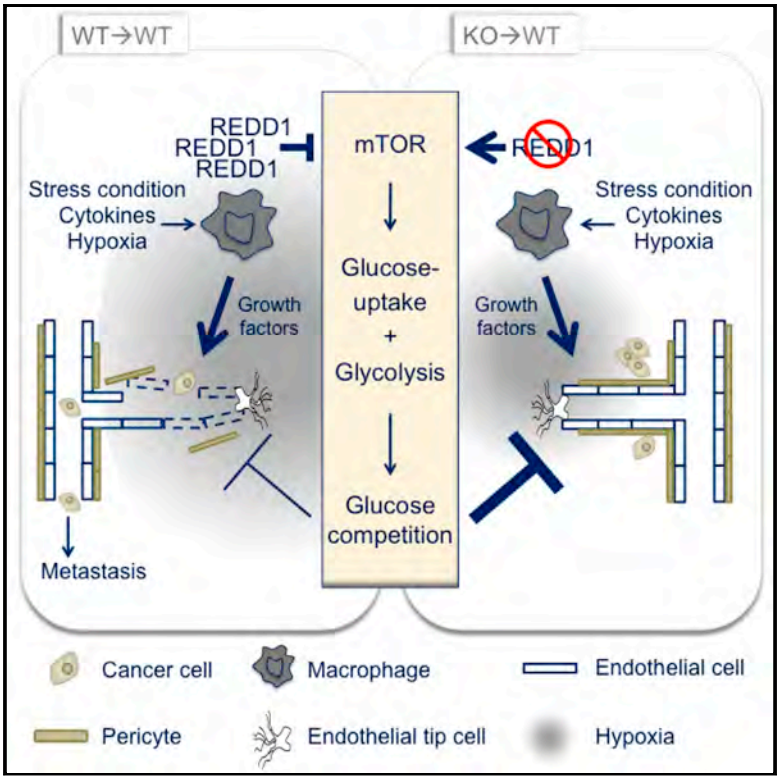

Highlights

- REDD1 deletion enhances glucose uptake and glycolysis in hypoxic TAMs via mTOR
- Enhanced glycolysis in REDD1 KO TAMs leads to glucose competition (GC) with tECs
- GC by REDD1 KO TAMs stabilizes tumor EC junctions and vessels preventing metastasis
- mTOR activation is antitumoral in hypoxic TAMs but protumoral in cancer cells

Authors

Mathias Wenes, Min Shang, Mario Di Matteo, ..., Bart Ghesquière, Peter Carmeliet, Massimiliano Mazzone

Correspondence

massimiliano.mazzone@vib-kuleuven.be

In Brief

Wenes et al. show that enhancing glycolysis via mTOR activation in hypoxic tumor-associated macrophages (TAMs) reduces endothelial glucose availability and promotes the formation of an organized tumor vasculature, which helps to restore oxygenation and prevent metastasis. The anti-tumor effects of mTOR inhibitors are mitigated by their effects on TAM metabolism.

Accession Numbers

E-MTAB-5032

Wenes et al., 2016, Cell Metabolism *24*, 1–15
November 8, 2016 © 2016 Elsevier Inc.
http://dx.doi.org/10.1016/j.cmet.2016.09.008

CellPress

Please cite this article in press as: Wenes et al., Macrophage Metabolism Controls Tumor Blood Vessel Morphogenesis and Metastasis, Cell Metabolism (2016), http://dx.doi.org/10.1016/j.cmet.2016.09.008

Cell Metabolism
Article

CellPress

Macrophage Metabolism Controls Tumor Blood Vessel Morphogenesis and Metastasis

Mathias Wenes,[1,2] Min Shang,[1,2] Mario Di Matteo,[1,2] Jermaine Goveia,[3,4] Rosa Martín-Pérez,[1,2] Jens Serneels,[1,2] Hans Prenen,[5] Bart Ghesquière,[6,7] Peter Carmeliet,[3,4] and Massimiliano Mazzone[1,2,8,*]
[1]Lab of Tumor Inflammation and Angiogenesis, VIB, 3000 Leuven, Belgium
[2]Lab of Tumor Inflammation and Angiogenesis, Department of Oncology, KU Leuven, 3000 Leuven, Belgium
[3]Lab of Angiogenesis and Vascular Metabolism, VIB, 3000 Leuven, Belgium
[4]Lab of Angiogenesis and Vascular Metabolism, Department of Oncology, KU Leuven, 3000 Leuven, Belgium
[5]Department of Digestive Oncology, University Hospitals Leuven and Department of Oncology, KU Leuven, 3000 Leuven, Belgium
[6]Metabolomics Expertise Center, VIB, 3000 Leuven, Belgium
[7]Metabolomics Expertise Center, Department of Oncology, KU Leuven, 3000 Leuven, Belgium
[8]Lead Contact
*Correspondence: massimiliano.mazzone@vib-kuleuven.be
http://dx.doi.org/10.1016/j.cmet.2016.09.008

SUMMARY

Hypoxic tumor-associated macrophages (TAMs) acquire angiogenic and immunosuppressive properties. Yet it remains unknown if metabolic changes influence these functions. Here, we argue that hypoxic TAMs strongly upregulate the expression of REDD1, a negative regulator of mTOR. REDD1-mediated mTOR inhibition hinders glycolysis in TAMs and curtails their excessive angiogenic response, with consequent formation of abnormal blood vessels. Accordingly, REDD1 deficiency in TAMs leads to the formation of smoothly aligned, pericyte-covered, functional vessels, which prevents vessel leakiness, hypoxia, and metastases. Mechanistically, highly glycolytic REDD1-deficient TAMs outcompete endothelial cells for glucose usage that thwarts vascular hyperactivation and promotes the formation of quiescent vascular junctions. Tuning down glycolysis in REDD1 knockout TAMs re-establishes abnormal angiogenesis and metastases. On this basis, we prove that the anti-tumor effect of mTOR inhibitors is partly countered by the deleterious outcome of these drugs on TAMs. Our data provide a functional link between TAM metabolism and tumor angiogenesis.

INTRODUCTION

Heterogeneity of macrophages has been long recognized as the result of the plasticity and versatility of these cells to different microenvironmental stimuli. In tumors, macrophages are involved in blood and lymphatic vessel formation, cancer cell invasion and distal dissemination, as well as immune suppression (Mantovani and Allavena, 2015). Recently, we have proved that tumor-associated macrophages (TAMs) within hypoxic niches of the tumor acquire a pro-angiogenic, pro-invasive, and tolerogenic phenotype (Casazza et al., 2013).

Hypoxic TAMs display strong alterations in the expression of several metabolic genes as they are forced to adapt their metabolism to low oxygen tension in order to meet their energy requirements (Laoui et al., 2014). Besides oxygen availability, cytokines also have an impact on macrophage metabolism, and different activation stimuli can drive opposing metabolic changes. For example, in vitro classically activated, pro-inflammatory M1 macrophages switch their metabolism toward enhanced anaerobic glycolysis, pentose phosphate pathway activation, and protein and fatty acid synthesis (Tannahill et al., 2013). On the other hand, alternative activation of macrophages by M2-inducing stimuli such as IL-4, IL-10, and IL-13 leads to a phenotype that more closely resembles the features of protumoral TAMs and is associated with enhanced oxidative phosphorylation, with no changes in glycolysis (Vats et al., 2006). Intriguingly, the metabolic characteristics of macrophages in the context of cancer have never been investigated, so it remains unknown if a change in TAM metabolism could influence their phenotype and thus affect cancer growth and metastasis.

The mechanistic target of rapamycin (mTOR) is a key nutrient and energy sensor that, on the basis of nutrient availability, regulates downstream metabolic processes such as glycolysis, de novo lipogenesis, protein synthesis, and transcription (Laplante and Sabatini, 2012). Hypoxia blocks mTOR function through HIF-mediated transcriptional induction of the mTOR complex 1 (mTORC1) inhibitor REDD1 (regulated in development and DNA damage response 1; otherwise known as RTP801 or DDIT4) (Brugarolas et al., 2004). Other than hypoxia, REDD1 is also induced by a variety of other stress conditions which are major features in cancer, including endoplasmic reticular stress (Wang et al., 2003), oxidative stress (Lin et al., 2005), osmotic stress (Wang et al., 2003), DNA-damaging agents (Ellisen et al., 2002), and cytokine stimulation such as IL-6 (Song et al., 2011).

Recent studies have shown that constitutive mTOR activation renders macrophages refractory to IL-4-induced M2 polarization, but increases inflammatory responses upon M1 stimuli (Byles et al., 2013). On the basis of the knowledge that hypoxia and stress conditions specifically control mTOR activity through REDD1 regulation, we hypothesized that the REDD1/mTOR

Please cite this article in press as: Wenes et al., Macrophage Metabolism Controls Tumor Blood Vessel Morphogenesis and Metastasis, Cell Metabolism (2016), http://dx.doi.org/10.1016/j.cmet.2016.09.008

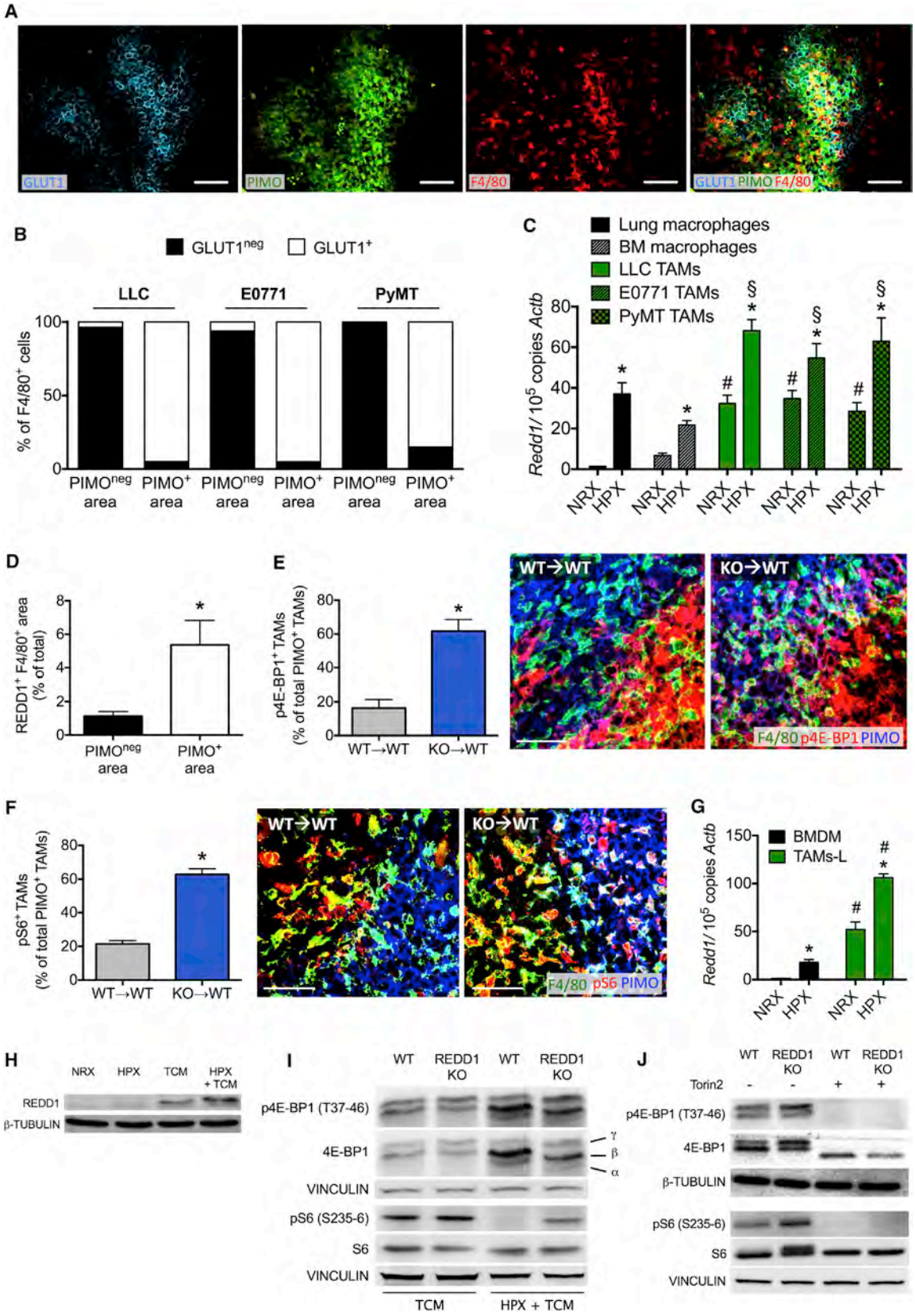

(legend on next page)

axis is a central homeostatic relay that links macrophage metabolism to the immunosuppressive and/or pro-angiogenic properties of hypoxic TAMs. Here, we studied the role of REDD1/mTOR in the control of macrophage and TAM metabolism in hypoxia and how this induces phenotypic changes that influence cancer progression.

RESULTS

REDD1 Is Upregulated in Hypoxic TAMs

A large body of evidence in several tumor types has proved that the induction of the hypoxia-responsive glucose transporter GLUT1 strongly and unequivocally correlates with oxygen shortage (Airley et al., 2003; Rademakers et al., 2011; Sennino et al., 2012). By looking at the pattern of GLUT1 and the hypoxia-probe pimonidazole in subcutaneous Lewis lung carcinomas (LLC), orthotopic E0771 breast cancer, and spontaneous PyMT mammary tumors, we confirmed that these two markers strongly overlapped and GLUT1^{+} TAMs were always positive for pimonidazole (Figures 1A and 1B). Thus, we sorted GLUT1^{high} (hypoxic) macrophages and GLUT1$^{low/-}$ (normoxic) macrophages from LLC, E0771, and PyMT tumors and healthy tissues (i.e., bone marrow [BM] or lung). Strikingly, the mRNA levels of *Redd1* were significantly higher in GLUT1^{high} versus GLUT1$^{low/-}$ tissue macrophages, while TAMs showed overall greater levels of *Redd1*, which was the highest in GLUT1^{high} TAMs (Figure 1C). In line, REDD1 staining in TAMs residing inside the hypoxic areas was much higher than in TAMs from the normoxic niches (Figure 1D). To dissect the contribution of hypoxia versus tumor-specific stimuli, we built an in vitro system in which BM-derived macrophages (BMDMs) were stimulated with LLC tumor-conditioned medium (TCM) as previously shown (Colegio et al., 2014; Finisguerra et al., 2015) and thus generated TAM-like macrophages (TAMs-L) that were exposed to normoxia or hypoxia. In this setting, several typical TAM markers followed a similar expression profile as LLC tumor-sorted TAMs (Figures S1A–S1J, available online). As in vivo, *Redd1* transcript and protein levels were both synergically increased when TAMs-L were cultured in hypoxia (Figures 1G and 1H). Overall, REDD1 is induced in TAMs (compared with normal macrophages) and gets strongly upregulated in hypoxia.

REDD1 Deletion in TAMs Promotes Tumor Vessel Normalization and Inhibits Metastasis

To understand the role of exacerbated REDD1 induction in hypoxic TAMs, we deleted *Redd1* in macrophages by transplanting wild-type (WT) recipient mice with REDD1 knockout (KO) BM cells (KO→WT). Upon reconstitution, KO→WT chimeras displayed normal blood counts, comparable with those of WT→WT mice (Table S1). We then implanted LLC tumors subcutaneously. Consistent with the inhibitory role of REDD1 on mTORC1, genetic deletion of *Redd1* re-established the phosphorylation of 4E-BP1 and S6 (respectively a direct and indirect mTOR target) in hypoxic TAMs (Figures 1E and 1F). In vitro, hypoxic, but not normoxic, REDD1 KO TAMs-L displayed also increased phosphorylation of 4E-BP1 and S6 (Figure 1I), and this induction was mTOR dependent (Figure 1J).

As an alternative to subcutaneous LLC tumors, we injected E0771 breast cancer cells orthotopically or we reconstituted 4-week-old PyMT mice in a C57BL/6 background with WT and REDD1 KO BM cells. In all three tumor models, *Redd1* deletion did not alter TAM accumulation nor their distribution in normoxic versus hypoxic niches (Figures S2A–S2C). Although tumor growth remained unchanged, the number of metastases in KO versus WT chimeric mice was decreased (Figures 2A–2I). Consistently, shedding of cancer cells from the primary tumor to the circulation was significantly impaired in KO→WT versus WT→WT LLC tumor-bearing mice (Figure 2J).

Hypoxic TAMs promote metastasis by influencing cancer cell motility and invasion and by facilitating cancer cell extravasation, survival, and growth at the metastatic site (Chen et al., 2011; Qian et al., 2011). However, LLC migration and collagen invasion in vitro were equally promoted by hypoxic WT and REDD1 KO TAMs (Figures S2D and S2E), and pulmonary lodging of cancer cells systemically injected into the bloodstream did not differ (Figure S2F). These data indicate that indirect mechanisms might be responsible for the reduced metastatic burden in tumor-bearing KO→WT mice.

Hypoxic TAMs repress T cells and sustain aberrant and dysfunctional tumor blood vessels (Henze and Mazzone, 2016). Although the numbers of tumor-infiltrating CD3^{+}CD4^{+} T-BET^{+} T_H1 cells, CD3^{+}CD4^{+}GATA3^{+} T_H2 cells, and CD3^{+}CD8^{+} T cells were comparable in both chimeras (Figures S2G–S2I), the tumor vascular trees were overtly different. As

Figure 1. REDD1 Upregulation in Hypoxic TAMs Suppresses mTOR Activity

(A) Representative images of GLUT1, pimonidazole (PIMO), and F4/80 staining (TAMs) in LLC tumors.

(B) Histological analysis indicating the percentage of F4/80^{+} TAMs that are either GLUT1 negative (GLUT1^{neg}) or GLUT1 positive (GLUT1^{+}) in normoxic (PIMO^{neg}) and hypoxic (PIMO^{+}) areas of LLC, E0771, or PyMT tumors. Total mice ten per tumor model.

(C) *Redd1* expression in CD11b^{+} F4/80^{+} macrophages sorted from normoxic (GLUT1$^{low/-}$, NRX) and hypoxic (GLUT1^{high}, HPX) regions of organs from healthy mice or tumors. Pooled data from two independent experiments, total mice four to seven per condition.

(D) Histological analysis of the percentage of REDD1 and F4/80-double positive area in normoxic PIMO^{neg} or hypoxic PIMO^{+} regions in LLC tumors.

(E and F) Histological analysis and representative images of the percentage of phospho-4E-BP1-positive (E) and phospho-S6-positive (F) F4/80^{+} TAMs in PIMO^{+} hypoxic regions of LLC tumors from lethally irradiated WT mice, transplanted with WT or REDD1 KO BM cells (WT→WT and KO→WT, respectively). Pooled data from two independent experiments, total mice ten per genotype.

(G and H) qRT-PCR (G) and western blot (H) for REDD1 on BMDMs treated for 18 hr in normoxia (21% O_2, NRX) or hypoxia (1% O_2, HPX) with or without tumor-conditioned medium (TCM).

(I) Western blot in BMDMs treated for 18 hr with TCM in normoxia (TCM) or hypoxia (HPX + TCM). The hyperphosphorylated γ-form of 4E-BP1 is indicated, which is unable to bind and inhibit the translation initiation factor eIF4E.

(J) Western blot in hypoxic WT and REDD1 KO TAMs-L, treated with or without 500 nM of the mTOR inhibitor Torin2.

*$p < 0.05$ versus NRX (C and G), PIMO^{neg} (D), or WT→WT (E and F); #$p < 0.05$ versus NRX lung and BM macrophages (C) or BMDM (G); §$p < 0.05$ versus HPX lung and BM macrophages. The scale bars represent 50 μm. All graphs show mean ± SEM. See also Figure S1.

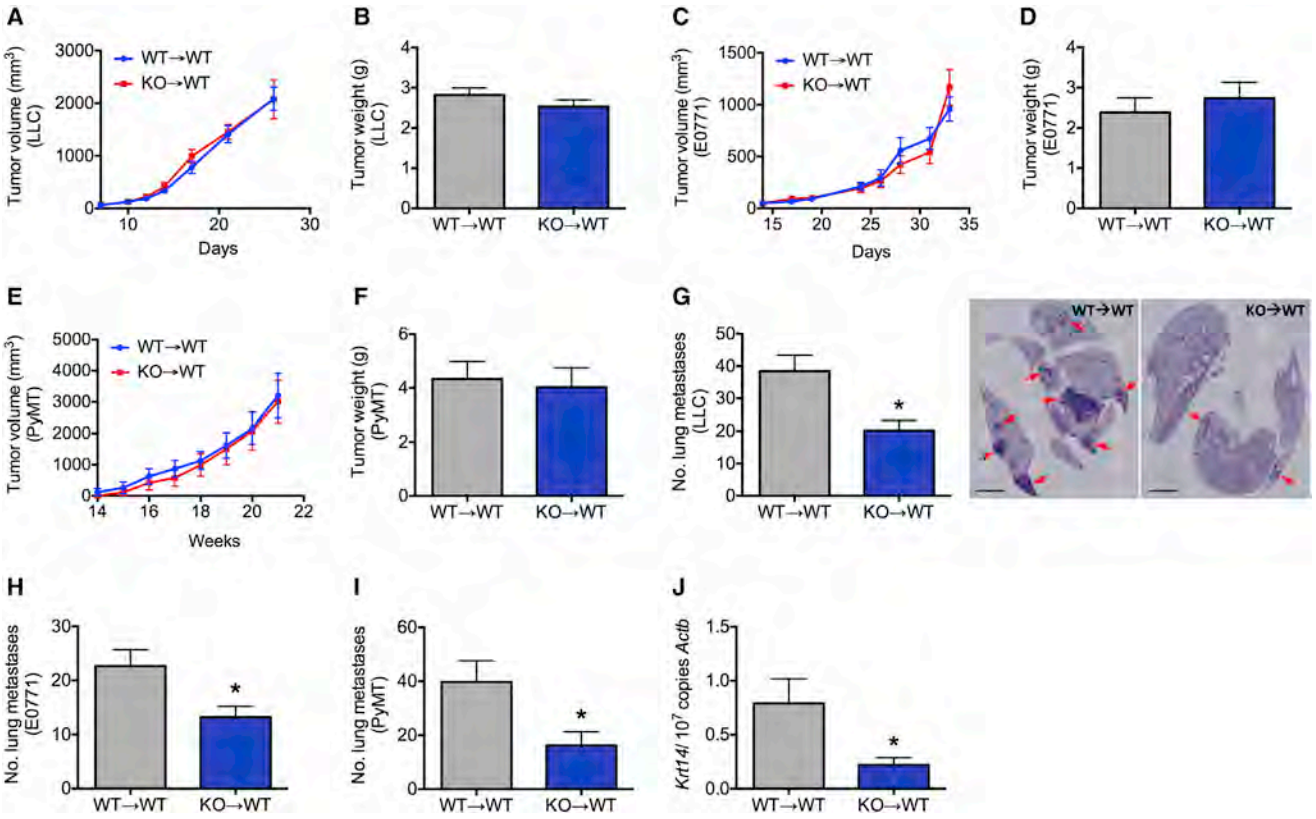

Figure 2. REDD1 Deletion in TAMs Inhibits Metastasis in Multiple Tumor Models

(A–F) Tumor growth (A, C, and E) and weight (B, D, and F) in the indicated tumor models.

(G–I) Lung metastatic nodules in LLC (G) (and representative H&E-stained lungs), E0771 (H), and PyMT (I) tumor-bearing mice. Data are pooled from three independent experiments, total mice 28 per genotype (LLC); from two independent experiments, total mice 18 per genotype (E0771); or from eight independent experiments, total mice 15 per genotype (PyVT).

(J) Circulating LLC cells, quantified by *Krt14* mRNA expression in the blood. Total mice 10 per genotype.

*$p < 0.05$ versus WT→WT. The scale bars represent 2 mm. All graphs show mean ± SEM. See also Figure S2 and Table S1.

expected, LLC tumor blood vessels in WT→WT mice had a disorganized, dilated appearance, with many protrusions. In contrast, the tumor vasculature in KO→WT mice displayed a smooth endothelial alignment and reduced vessel diameter (Figure 3A). Similar features of vascular normalization were found in the orthotopic E0771 breast cancer model as well as in the PyMT-driven spontaneous breast cancer model (Figures 3B and 3C). Tumor vessels of KO→WT mice were more covered with pericytes (Figures 3D–3F) and had more abundant vascular endothelial (VE)-cadherin junctions (Figure 3G), which together provide stability and tightness to the blood vessel barrier (Mazzone et al., 2009; Xian et al., 2006). Functionally, this resulted in improved perfusion, lower vascular permeability, and reduced tumor hypoxia (Figures 3H–3N) despite comparable vessel density (Figures S2J–S2L). These morphological and functional tumor vascular changes have been already shown to reduce metastasis (Maes et al., 2014; Mazzone et al., 2009; Rolny et al., 2011).

To reinforce the evidence that REDD1-deficient TAMs were the main contributors to the observed phenotype, we depleted macrophages in WT→WT and KO→WT mice by intraperitoneal (i.p.) administration of an anti-CSF-1R blocking antibody (clone AFS98), which resulted in about 90% reduction in TAM density in both genotypes (Figure 4A). As expected (Rolny et al., 2011), TAM depletion reduced both tumor growth and metastasis in a WT context, but this treatment did not further reduce metastatic growth in REDD1 KO chimeras compared with mice treated with an IgG control (Figures 4B and 4C). Following anti-CSF-1R treatment, the tumor vasculature in WT chimeric mice resembled the same features observed in REDD1 KO→WT mice, whereas TAM depletion in the latter mice did not further impinge on tumor vessels (Figures 4D–4G), altogether arguing that the effect of hematopoietic REDD1 deletion on metastasis and blood vessels reflects mostly a change in TAMs and not in other hematopoietic cells.

Metastases were also prevented when LLC tumors were grown in non-transplanted REDD1 KO mice (in which all stromal cells including the endothelium itself are deficient for *Redd1*) (Figure 4H), with increased vessel functionality (Figures 4I and 4J). These data exclude the possibility that all the aforementioned data are related to a specific condition triggered by whole-body irradiation prior to transplantation (Ahn and Brown, 2008) and further support the prominent role of REDD1 in inflammatory cells, rather than in other stromal components. In

conclusion, deficiency of REDD1 in TAMs promotes vessel normalization and reduces metastasis in several tumor types.

REDD1 Deletion in Hypoxic TAMs Reinforces Glycolysis

By performing metabolic assays, we observed that hypoxic TAMs showed an increase in glycolysis (Figure 5A). However, upon *Redd1* deletion, the glycolytic flux was further increased in an mTOR-dependent manner (Figure 5A).

In turn, fatty acid oxidation (FAO) was decreased in hypoxic REDD1 KO TAMs, while glucose and glutamine oxidation remained unchanged (Figures 5B–5D). When this was translated in terms of ATP production, we observed an equal balance in glycolytic versus mitochondrial contribution to the ATP pool in hypoxic WT TAMs (Figure 5E). Differently, in hypoxic REDD1 KO TAMs, glycolysis was the main contributor to the ATP pool, a characteristic of in vitro polarized M1 macrophages (Rodríguez-Prados et al., 2010), whereas the percentage of ATP molecules from fatty acid oxidation, a characteristic of M2 macrophages, was reduced so that the total ATP levels and energy charge remained unchanged (Figures 5F and 5G). Although also reduced in hypoxic versus normoxic WT cells, ATP-linked mitochondrial oxygen consumption reached the lowest levels in hypoxic (GLUT1^{high}) REDD1 KO TAMs, and this difference was mTOR dependent (Figure 5H). In vitro analysis showed that only the combined induction of REDD1 by hypoxia and tumor-derived stimuli in the TCM (but not each in condition alone) was able to effectively brake glycolytic metabolism (Figures 5I and 5J).

When looking at normoxic TAMs, *Redd1* deficiency did not alter either glycolysis or the contribution of the four major fluxes (glycolysis, glucose oxidation, glutamine oxidation, and FAO) to the ATP pool (Figures 5A and 5K) opening the question if REDD1 in the more oxidative (GLUT1$^{low/-}$) TAM fraction might play a role in the control of mitochondrial ROS formation (Horak et al., 2010).

In line with the observed increase in glycolysis, hypoxic REDD1 KO TAMs (but not the normoxic ones) showed the highest levels of GLUT1, which was accompanied by a strong increase in glucose uptake (Figures 5L–5N). Similarly, GLUT1 expression and glucose uptake was enhanced in hypoxic REDD1 KO TAMs-L when compared with hypoxic WT TAMs-L (Figures 5O and 5P). Both in TAMs and in TAMs-L, this induction was dependent on mTOR (Figures 5N and 5O).

Altogether, REDD1 deletion in hypoxic TAMs reinforces their glycolytic phenotype at the expense of oxidative pathways, and in particular of FAO, via mTOR activation.

Increased Glycolysis in REDD1 KO TAMs Causes Tumor Vessel Normalization by Competing for Glucose with Endothelial Cells

In the attempt to understand how the metabolic changes observed in hypoxic (GLUT1^{high}) TAMs could influence their phenotype, we performed RNA sequencing on WT and REDD1 KO CD11b^{+} F4/80^{+} GLUT1^{high} macrophages sorted using fluorescence-activated cell sorting (FACS) from LLC tumors (ArrayExpress: E-MTAB-5032). In general, only five genes were differentially expressed (Benjamini-Hochberg adjusted $p < 0.05$) (Table S2). Heatmap analysis of M1 and M2 gene expression (Mantovani et al., 2002; Mosser and Edwards, 2008; Sica and Mantovani, 2012) did not reveal distinct signatures in WT versus REDD1 KO GLUT1^{high} TAMs or in WT versus REDD1 KO GLUT1$^{low/-}$ TAMs (Figures S3A and S3B). Accordingly, histological analysis and FACS quantifications could not uncover an imbalance in TAM subsets (Figures S3C–S3F). In a similar fashion, while self-contained gene set enrichment analysis showed that a predefined angiogenic gene signature (Mazzieri et al., 2011; Murdoch et al., 2008) was significantly upregulated in GLUT1^{high} TAMs as compared with Glut1$^{low/-}$ TAMs ($p = 0.0001$), GLUT1^{high} and Glut1$^{low/-}$ KO TAMs did not differ from their WT counterparts (Figure S3G). We then hypothesized that enhanced glucose uptake and consumption by REDD1 KO GLUT1^{high} TAMs could install a competition with tumor endothelial cells (tECs) for their more important fuel (De Bock et al., 2013). Of relevance, in a tumor, per each endothelial cell (EC), there are about 20 TAMs, so that the weight of metabolic differences in TAMs is suddenly increased by the large representation of these cells (our data in LLC tumors, Figure S4A; Shigeoka et al., 2013; Takeuchi et al., 2016). Interestingly, in WT→WT mice, glucose uptake by tECs was twice the uptake measured in TAMs (Figure 6A). In contrast, in KO→WT mice, TAMs and tECs had similar glucose uptake, reflecting stronger glucose uptake by REDD1 KO versus WT TAMs, which goes at the expense of endothelial glucose consumption, as proved by the fact that TAM depletion abolished this trend (Figure 6A).

Previous data have shown that glycolysis blockade renders ECs more quiescent, and this is due mostly to the influence of cytosolic ATP on cytoskeleton rearrangements that in turn are associated with the redistribution of cell-cell contacts (De Bock et al., 2013). Because the in vivo data showed an alteration in endothelial junctions without a difference in vessel numbers (nor in EC survival or apoptosis; Figures S4B and S4C), we focused our attention on this parameter by using in vitro assays. We first seeded WT and REDD1 KO TAMs-L in the lower part of a Boyden chamber and placed a confluent layer of human umbilical vein ECs (HUVECs) on the upper side of a 0.4-μm-pore filter (that allows molecule exchange but impedes cell migration). In the presence of WT TAMs-L, VE-cadherin junctions displayed a rope ladder-like pattern (which is typical of an activated endothelium; Bentley et al., 2014), while in presence of REDD1 KO TAMs-L, VE-cadherin was linearly distributed along the cell-cell junction, which is a sign of stability (Figures 6B and 6C). In the presence of higher glucose (5.5 mM instead of 0.6 mM, roughly corresponding to the concentrations of glucose in circulation and in the tumor; Ho et al., 2015), VE-cadherin junctions were activated independently of the presence of WT or REDD1 KO TAMs-L (Figures 6B and 6C). Functionally, only in low glucose, the presence of REDD1 KO TAMs-L was associated with increased transendothelial electrical resistance (TEER), which is in line with the tighter endothelial barrier observed in vivo (Figure 6D).

To verify if the increase in glycolysis or glucose uptake in REDD1 KO TAMs was the underlying cause of the observed phenotype, we sought to delete in macrophages only, both *Redd1* and *Pfkfb3*, a key glycolytic activator responsible for enhanced glycolysis and reduced oxygen consumption in REDD1 KO TAMs (Figures S4D and S4E). Therefore, we intercrossed REDD1 KO mice with *Pfkfb3*$^{lox/lox}$x*Csf1r.Mer2.Cre*

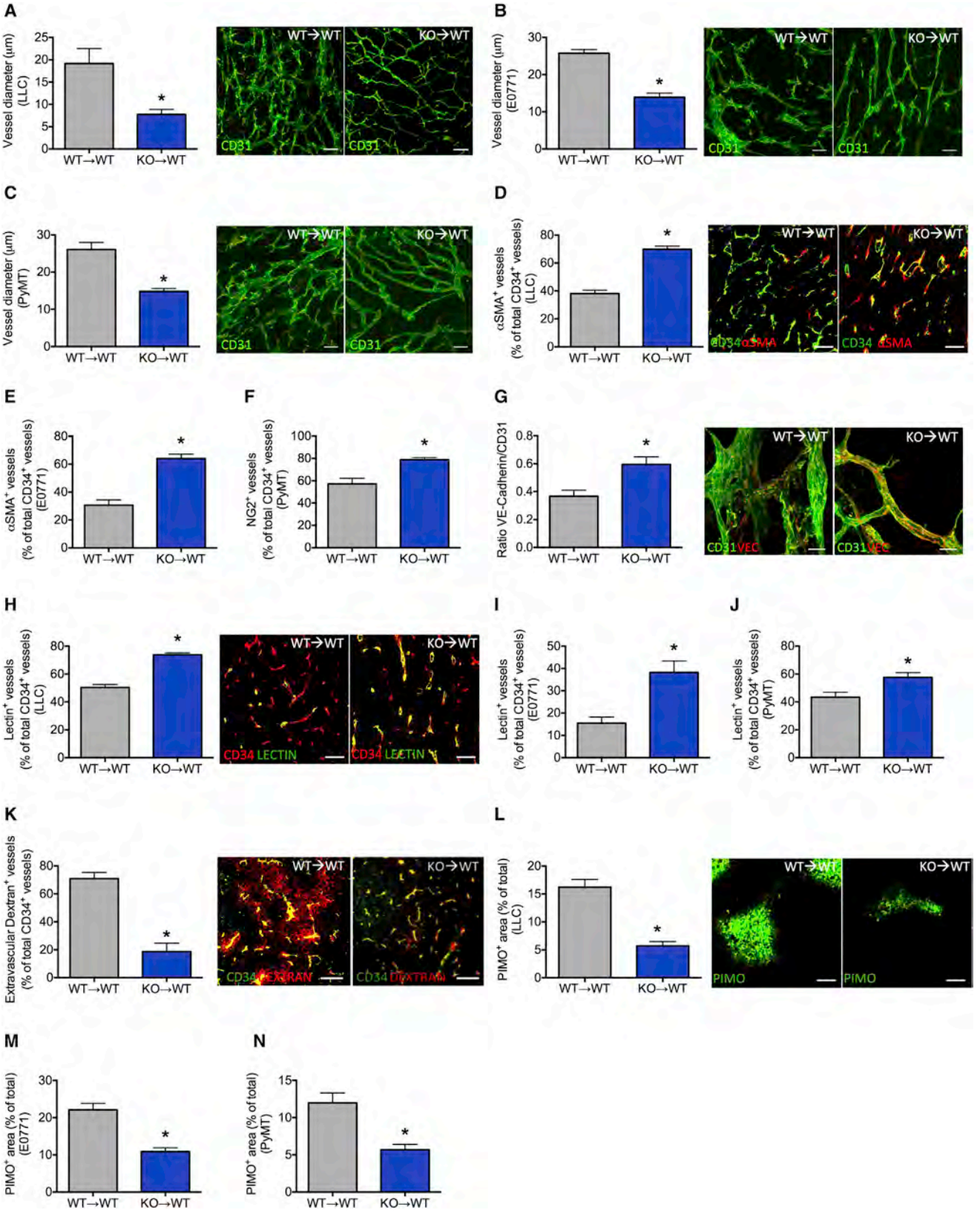

(legend on next page)

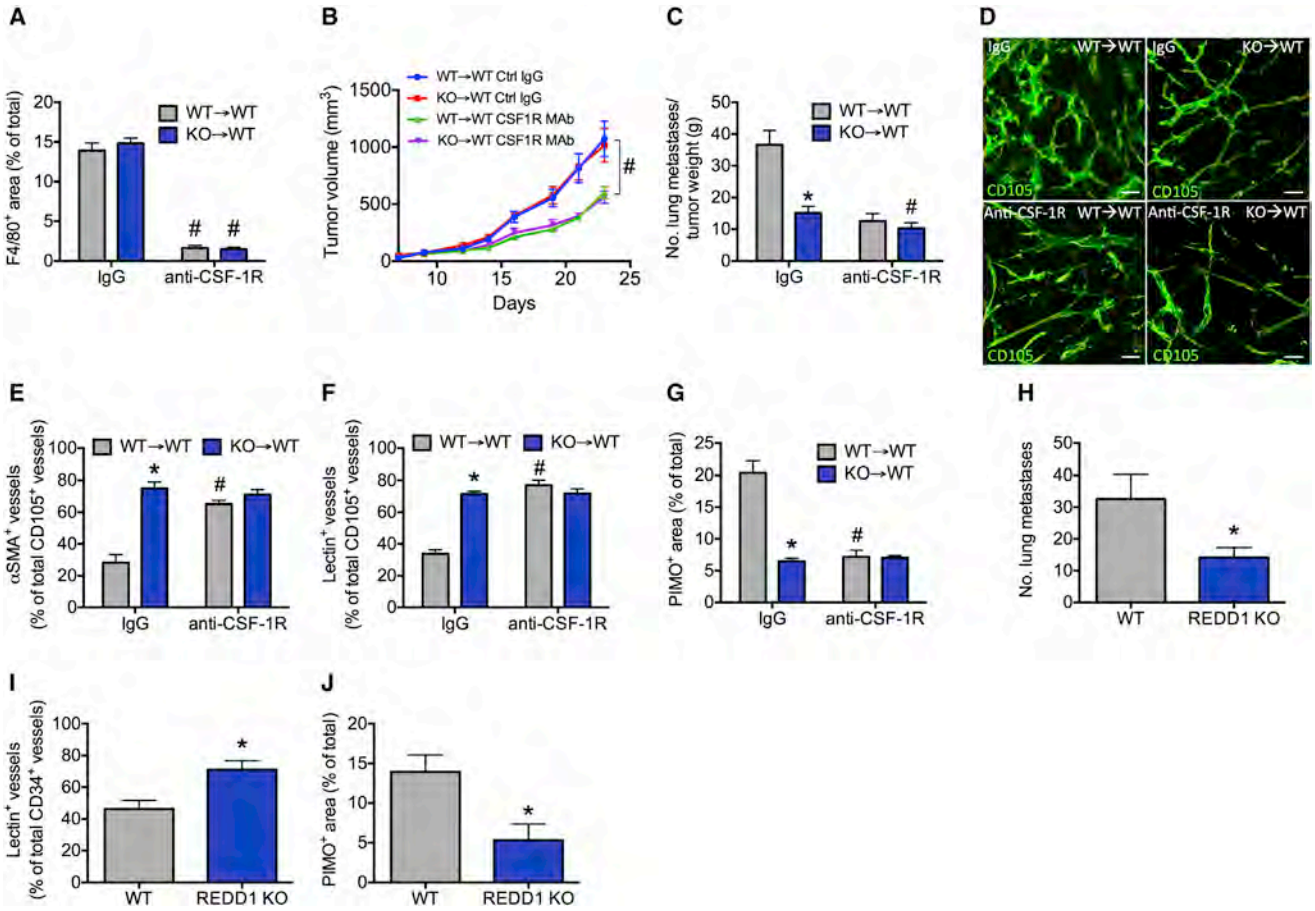

Figure 4. Macrophage Depletion Abrogates the Vascular and Metastatic Differences Induced by REDD1 Deletion in TAMs

(A) F4/80$^+$ macrophage accumulation in LLC tumors of mice treated with control IgG isotype or TAM-depleting anti-CSF-1R monoclonal antibodies.

(B and C) LLC tumor growth (B) and metastatic index (C).

(D) Representative confocal images of CD31$^+$ blood vessel morphology.

(E–G) Pericyte coverage (E), blood vessel perfusion (F), and tumor hypoxia (G). Total mice 8–10 per condition.

(H) Metastatic nodules in lungs of non-transplanted LLC tumor-bearing mice.

(I and J) Blood vessel perfusion (I) and tumor hypoxia (J) in non-transplanted LLC tumor-bearing mice. Total mice 7 per genotype.

*$p < 0.05$ versus WT→WT or WT; #$p < 0.05$ versus IgG. The scale bars represent 50 μm. All graphs show mean ± SEM.

mice, the latter enabling tamoxifen-inducible, macrophage-specific deletion of *Pfkfb3* (Figure S4F; Chesney et al., 2005; Qian et al., 2011). In subcutaneously grown LLC tumors, PFKFB3 deletion in REDD1 KO TAMs (REDD1$^{bm\Delta}$PFK$^{mo\Delta}$) resulted in an abnormal vasculature, similar to that found in tumors in which TAMs were WT for both genes (Figure 6E). Indeed, tumor blood vessels in REDD1$^{bm\Delta}$PFK$^{mo\Delta}$ mice were sparsely covered with pericytes and poorly perfused, leading to persistent hypoxia (Figures 6F–6K). Of note, PFKFB3 deletion altered neither TAM infiltration nor vessel density (Figures S4G and S4H). Concomitant with the abnormal tumor vasculature and increased hypoxia, PFKFB3 deletion abrogated the protective effect of

Figure 3. REDD1 Deletion in TAMs Promotes Tumor Blood Vessel Normalization

(A–C) CD31$^+$ blood vessel morphology in the indicated tumor models, quantification of vessel diameter, and representative maximum intensity projection images from confocal Z-stacks acquired on 80-μm-thick sections.

(D and E) Percentage of αSMA$^+$ pericyte-covered vessels over the total number of CD34$^+$ vessels acquired on thin sections of LLC tumors (D, and representative images) and E0771 tumors (E).

(F) Percentage of NG2$^+$ pericyte-covered vessels in PyMT tumors.

(G) Ratio of VE-cadherin (VEC) to CD31 staining and representative confocal images of thick LLC tumor sections.

(H–J) Percentage of lectin-FITC$^+$ perfused vessels in LLC (H, and representative images), E0771 (I), and PyMT tumors (J).

(K) Quantification and representative images of the percentage of 70 kDa dextran$^+$ leaky vessels in LLC tumors.

(L–N) Percentage of pimonidazole-positive hypoxic area acquired in LLC (L, and representative images), E0771 (M), and PyMT tumors (N). Data are pooled from three independent experiments, total mice 28 per genotype (LLC); from two independent experiments, total mice 18 per genotype (E0771); or from eight independent experiments, total mice 15 per genotype (PyVT).

*$p < 0.05$ versus WT→WT. The scale bars represent 10 (G) or 50 μm (A–D, H, K, and L). All graphs show mean ± SEM. See also Figure S2.

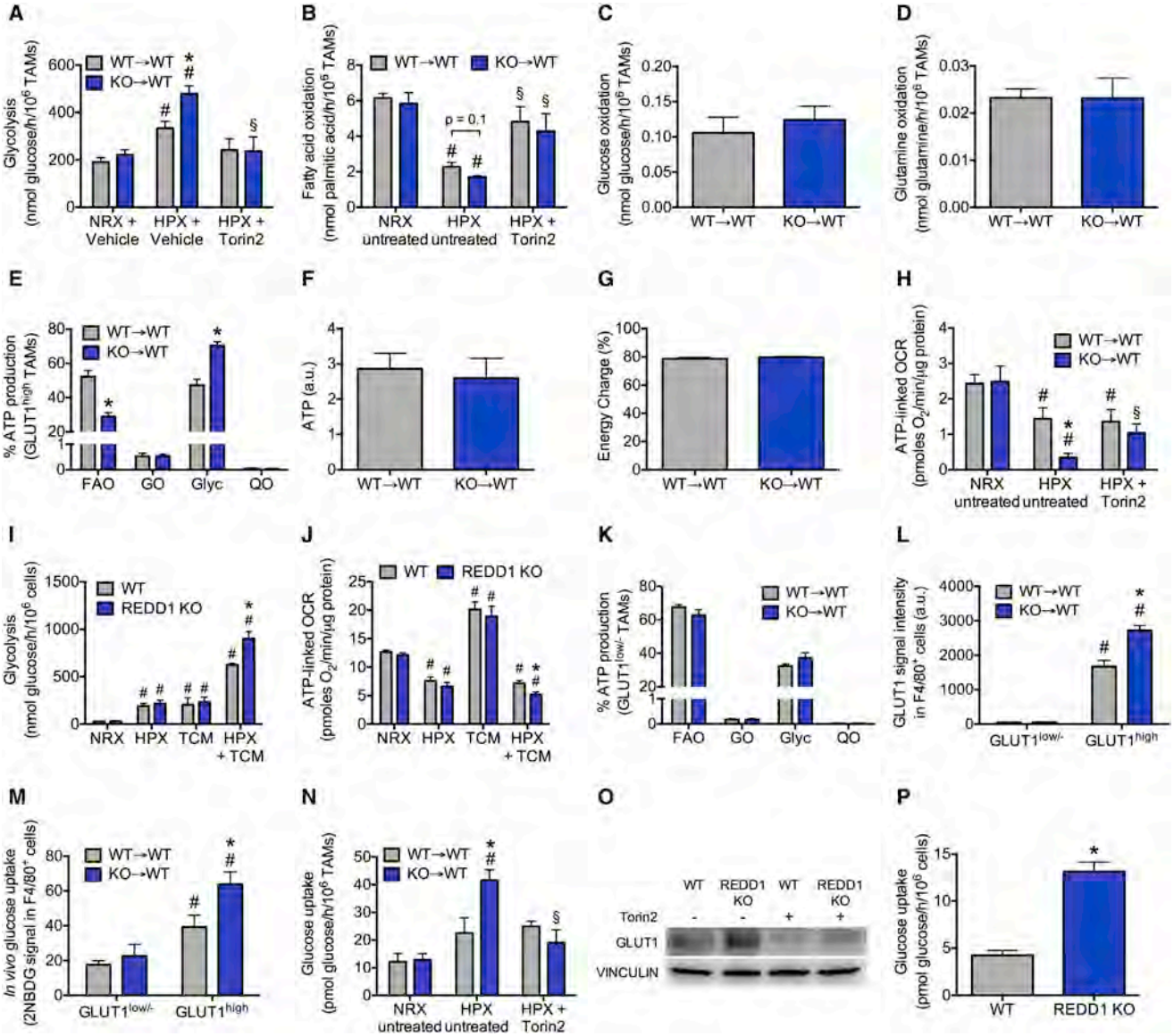

Figure 5. REDD1 Expression in Hypoxic TAMs Limits Their Glycolytic Metabolism

(A) Glycolytic flux in GLUT1$^{low/-}$ (NRX) and GLUT1^{high} (HPX) CD11b^{+} F4/80^{+} TAMs, sorted using FACS from LLC tumors treated with Torin2 or vehicle.

(B) Fatty acid oxidation in TAMs treated or not ex vivo with 100 nM Torin2.

(C and D) Glucose (C) and glutamine (D) oxidation in GLUT1^{high} CD11b^{+} F4/80^{+} TAMs.

(E) Flux analysis showing the contribution of fatty acid oxidation (FAO), glucose oxidation (GO), glycolysis (Glyc), and glutamine oxidation (QO) in percentage of the total cellular ATP pool in hypoxic GLUT1^{high} CD11b^{+} F4/80^{+} TAMs.

(F and G) LC-MS measurement of total cellular ATP content (F) and energy charge ([ATP] + 1/2[ADP]/[ATP] + [ADP] + [AMP]) (G) in F4/80^{+} TAMs.

(A–G) Pooled data from two independent experiments, total mice six per genotype in technical triplicates.

(H) Oxygen consumption rate (OCR) in TAMs, treated or not ex vivo with Torin2. Total mice three per genotype in technical triplicates.

(I and J) Glycolysis and OCR in REDD1 WT and KO BMDMs treated for 18 hr in normoxia (21% O_2, NRX) or hypoxia (1% O_2, HPX) with or without TCM. Representative graphs from two independent experiments, total mice six per genotype in technical triplicates.

(K) Flux analysis in normoxic GLUT1$^{low/-}$ CD11b^{+} F4/80^{+} TAMs. Total mice six per genotype in technical triplicates.

(L) FACS analysis of GLUT1 mean signal intensity in GLUT1$^{low/-}$ and GLUT1^{high} F4/80^{+} TAMs.

(M) Glucose uptake in TAMs measured by FACS quantification of the signal intensity of a fluorescently labeled glucose analog (2NBDG) in GLUT1$^{low/-}$ and GLUT1^{high} F4/80^{+} macrophages, injected intratumorally. Total mice six per genotype.

(N) ^{14}C-2-deoxyglucose uptake in TAMs, treated or not ex vivo with Torin2. Total mice three per genotype in technical triplicates.

(O) Western blot for GLUT1 in hypoxic TAMs-L treated with or without Torin2. Representative of two independent experiments.

(P) ^{14}C-2-deoxyglucose uptake in hypoxic TAMs-L. Pooled data from three independent experiments, total mice six per genotype in technical triplicates.

*p < 0.05 versus WT→WT or WT; #p < 0.05 versus NRX or GLUT1$^{low/-}$; §p < 0.05 versus HPX + vehicle or HPX untreated. All graphs show mean ± SEM.

REDD1 deletion in TAMs on metastatic dissemination, despite tumor growth, remained unaffected (Figures 6L–6N). Reduction of glucose consumption by REDD1$^{bm\Delta}$PFK$^{mo\Delta}$ TAMs increased endothelial glucose uptake to the same levels as in REDD1^{wt}PFK^{wt} mice (Figure 6O). In conclusion, increased glycolysis upon deletion of REDD1 in hypoxic TAMs brings these cells in competition for glucose with the tumor endothelium. As a result, lower glucose availability in the perivascular space thwarts endothelial hyperactivation, which leads to vascular stabilization and metastasis inhibition (Figure 6P).

Opposite Role of mTOR Pathway in Cancer Cells and TAMs

Pharmacologic inhibition of mTOR has been proposed in the clinic because of the relevance of this pathway in boosting protein synthesis and cancer cell proliferation (Don and Zheng, 2011; Hsieh et al., 2012). According to the aforementioned data, however, mTOR activation would unleash tumor-inhibiting functions in TAMs. To validate this hypothesis, we administered Torin2 to WT→WT and KO→WT tumor-bearing mice. Although tumor growth inhibition by Torin2 was comparable in both chimeras, metastatic index was boosted up to the same levels so that REDD1 deficiency in TAMs was no longer beneficial (Figures 7A and 7B). This phenotype was associated by increased tumor vessel abnormalization and hypoxia in Torin2-treated WT→WT and KO→WT mice, which were now comparable (Figures 7C–7F). To dissect the effect of mTOR inhibition in cancer cells and in the tumor stroma, we compared the outcome of mTOR silencing in LLC cells (Figure S5A) versus systemic administration of Torin2. Torin2 decreased the volume of LLC tumors by 30% and mTOR knockdown in cancer cells by 70% (Figure 7G). However, the effect of combined mTOR silencing and systemic Torin2 administration was not additive but conversely re-established tumor growth almost at the same level as observed with Torin2 alone (Figure 7G). As expected, mTOR silencing in cancer cells reduced metastases, whereas systemic Torin2 treatment drastically increased metastases, thereby blunting the beneficial effects of mTOR silencing in LLC cells (Figure 7H). Accordingly, normalized blood vessels and reduced hypoxia upon mTOR silencing in LLC cells was abrogated by systemic Torin2 treatment (Figures 7I–7L). Of note, blood vessel density was equally reduced in all treatment groups (Figure S5B), most likely because of reduced VEGF production after mTOR inhibition in the cancer cells, as already described (Guba et al., 2002). To restrict the effect of mTOR inhibition to the TAMs (and not to other stromal cells), we proposed Torin2 administration in combination with the TAM-depleting antibody anti-CSF-1R. In this setting, while Torin2 and anti-CSF-1R together additively inhibited tumor growth (Figure 7M), the metastatic boost observed with systemic Torin2 alone was greatly prevented when combined with TAM depletion (Figure 7N). Accordingly, the increase in vessel abnormalization and tumor hypoxia upon Torin2 treatment was partially reversed as well (Figures 7O–7R). Thus, the anti-tumor effect of systemic mTOR inhibition occurs mainly through the inhibition of this pathway in cancer cells, while it is partly countered by the effect on TAMs in which, contrary to REDD1 knockout and mTOR activation, mTOR blockade further sustains tumor vessel abnormalization and metastasis.

DISCUSSION

So far, the intertwined relationship between metabolism and macrophages in the context of cancer is completely unexplored. Starting from our previous observations that hypoxic TAMs acquire pro-angiogenic and immune suppressive features (Casazza et al., 2013), we now show that REDD1, a negative regulator of mTORC1 (Brugarolas et al., 2004), reaches the highest level of induction in response to tumor hypoxia, and we suggest that this induction plays a key role in the metabolic switch of hypoxic TAMs and in turn on tumor oxygenation and vascularization.

When preventing TAMs' entry into the hypoxic regions of the tumor, the contributions of these cells to cancer cell spreading, angiogenesis, and immunosuppression are all affected (Casazza et al., 2013; Laoui et al., 2014). The present data suggest that metabolic changes dictated by REDD1-mediated mTOR inhibition in TAMs specifically affect vascular remodeling and oxygen delivery without modulating the influence of TAMs on cancer cell invasion or on the immune system. In support of this idea, specific knockout of PFKFB3 in macrophages, restoring the glycolytic flow of REDD1 KO TAMs to WT levels, prevents tumor blood vessel normalization without altering vessel density or tumor growth. The effect of this metabolic rewiring on vessel morphogenesis is due mostly to enhanced glucose uptake and glycolysis by the hypoxic TAMs that install a competition with tECs, which in response to lower glucose rewire their phenotype toward quiescence and engage stable cell-cell junctions. It remains to be addressed if other tumor cells besides the endothelium (e.g., pericytes or cancer cells) enter into competition with TAMs for their fuel. Likely, glucose competition occurs also in a WT context in which, however, the surge of TAM-derived angiogenic cues prevails, as suggested by the fact that TAM depletion normalizes the tumor vasculature. By genetic means, the capacity of TAMs to compete for glucose with tECs is enhanced to a level that it counters the overall angiogenic burst of the tumor environment.

A possible question that derives from our work is how hypoxic TAMs can have access to the glucose coming from the blood. Likely, the glucose in circulation (which normally diffuses for longer distances than oxygen; Gatenby and Gillies, 2004) can reach the hypoxic TAMs because neoplastic cells at the vascular rim oxidize lactate (instead of glucose) in favor of hypoxic and glycolytic cancer cells (Allen et al., 2016).

Previous literature has shown that mTOR hyperactivation after genetic deletion of its negative regulator TSC1 hinders M2-like responses to IL-4 or other M2 stimuli (Byles et al., 2013; Zhu et al., 2014), whereas pharmacologic mTOR inhibition promotes an anti-inflammatory M2 phenotypic shift (Han et al., 2016). The present study moves the field forward and sheds light into the metabolic control by the REDD1-mTOR pathway in TAMs. In line with our previous findings that hypoxia per se does not change the ratio between different TAM subsets (Laoui et al., 2014), a metabolic change in hypoxic TAMs only fine-tunes the angiogenic properties of TAMs without altering the accumulation of distinct M1- or M2-like subpopulations and without altering the actual balance between pro-angiogenic (M2) versus anti-angiogenic (M1) cytokines. Instead, mTOR activation by REDD1 deletion enhances the expression of the main glucose transporter GLUT1 and reinforces glucose uptake. A previous

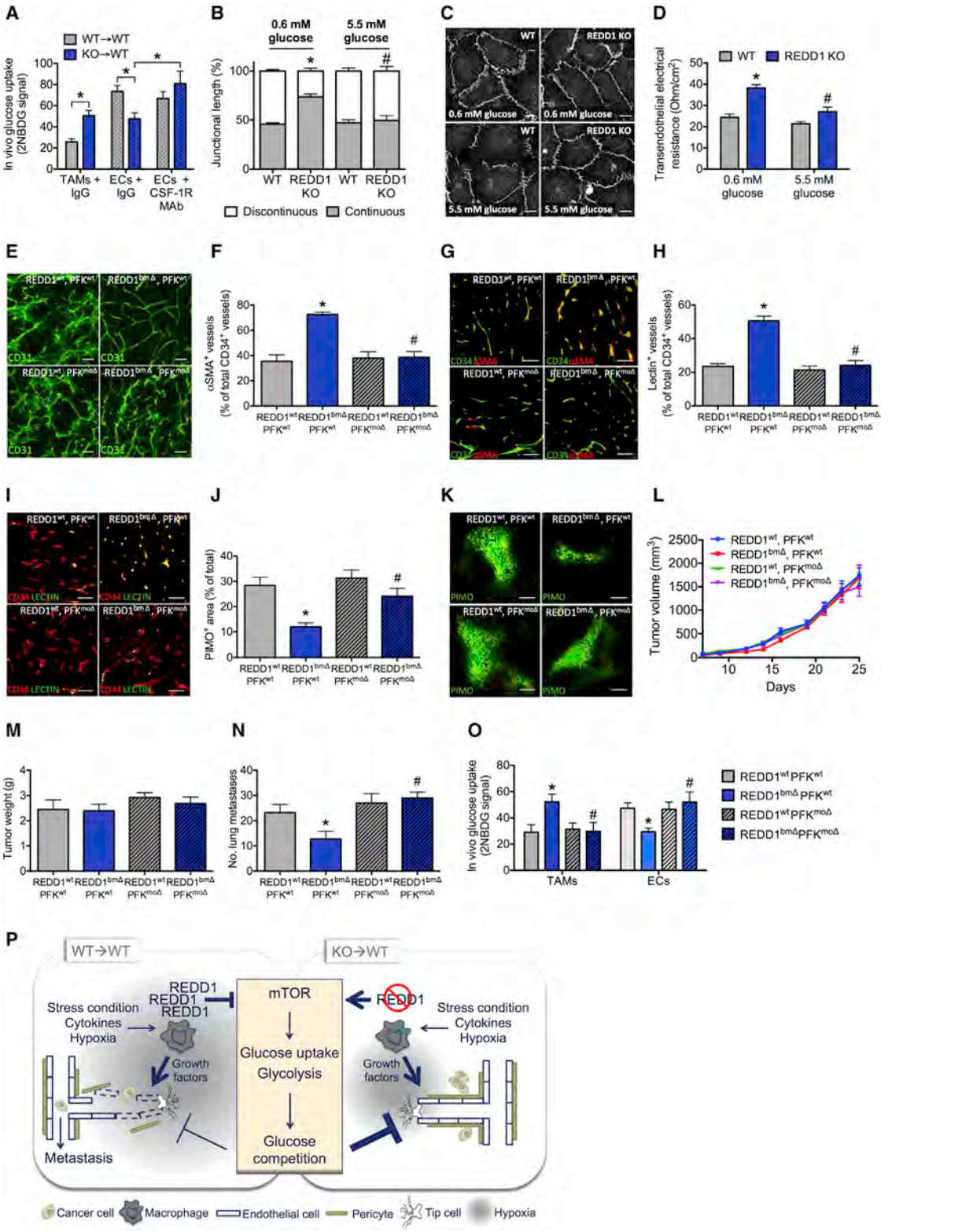

Figure 6. Increased Glycolysis in REDD1 KO TAMs Causes Tumor Vessel Normalization by Competing for Glucose with ECs

(A) In vivo 2NBDG glucose uptake in F4/80⁺ macrophages and CD31⁺ ECs, in mice treated with control IgG isotype or TAM-depleting anti-CSF-1R monoclonal antibodies. Total mice six per condition.

(legend continued on next page)

study has already shown that GLUT1 overexpression in macrophages is sufficient to enhance glycolysis (Freemerman et al., 2014). On this basis, and given the evidence that mTORC1-mediated phosphorylation of 4E-BP1 results in its inhibition and consequently in the block of *Glut1* mRNA translation (Taha et al., 1999), we suppose that the observed effects on GLUT1 protein levels and glucose uptake in REDD1 KO TAMs (and TAMs-L) are mediated, at least in part, by 4E-BP1.

During physiological processes such as embryogenesis and organ formation, macrophages are known to display an important pro-angiogenic function (Fantin et al., 2010; Stefater et al., 2011). Our results suggest that hypoxic upregulation of REDD1 in normal situations is dispensable as REDD1 KO mice are normal and do not show overt pathological signs. However, under stress conditions and in combination with tumor-derived stimuli, REDD1 is induced beyond proportions. As a consequence, deletion of REDD1 in the hypoxic TAMs remarkably upregulates glucose competition so that the blood vessels become smoothly aligned, tightly connected, and well-covered by pericytes. Tumor oxygenation and vessel coverage together prevent metastasis formation (Figure 6P).

Because hyperactivation of mTOR signaling is found in many cancers and given that alterations in the mTOR pathway are associated with cancer development and progression (Hsieh et al., 2012; Sun et al., 2015), mTOR inhibitors provide therapeutic value in a number of cancers, in both preclinical and clinical settings (Don and Zheng, 2011; Li et al., 2014). Interestingly, in PTEN-deficient glioblastomas, the mTOR inhibitor rapamycin reduces cancer cell proliferation and improves clinical outcomes in 50% of the patients (Cloughesy et al., 2008). In those patients who do not respond, cancer cells remain in any case sensitive to rapamycin in vitro, suggesting that resistance is likely due to cancer cell-extrinsic mechanisms. Following these observations and on the basis of the present findings, a possible future study could aim to look at REDD1^{+} TAMs in correlation with treatment failures of rapalogs and other mTOR-targeting drugs.

Altogether, our results establish a causative link between TAM metabolism in hypoxia and tumor vessel morphogenesis.

EXPERIMENTAL PROCEDURES

More detailed methods can be found in the Supplemental Experimental Procedures.

Animals

REDD1 KO mice were generated by Lexicon exclusively for Quark Pharmaceuticals and are the property of Quark Pharmaceuticals. *Pfkfb3*$^{lox/lox}$ were provided by J. Chesney (University of Louisville). *Csf1r.Mer2.Cre* mice were obtained from J. Pollard (University of Edinburgh). C57BL/6 and FVB MMTV-PyMT mice were purchased from Harlan and Charles River, respectively. FVB MMTV-PyMT mice were then backcrossed in a C57BL/6 background in our facility. Acute deletion of PFKFB3 was obtained by i.p. injection of tamoxifen (1 mg/mouse/day) for 5 days before subcutaneous implantation of LLC cancer cells. All mice used were on a C57BL/6 background and between 5 and 15 weeks old, without specific gender selection. In all experiments, littermate controls were used.

Bone Marrow Transplantation

Five- to 6-week-old C56BL/6 or 3- to 4-week-old PyMT recipient mice were irradiated with 9.5 Gy. Subsequently, 10^7 bone marrow cells from the appropriate genotype were injected intravenously via the tail vein. Tumor experiments were initiated 5 weeks after bone marrow reconstitution.

Tumor Models

Housing and all experimental animal procedures were approved by the Institutional Animal Care and Research Advisory Committee of the KU Leuven. LLC cells (1×10^6) were injected subcutaneously or 5×10^5 E0771 cells were injected orthotopically in the mammary fat pad. Circulating cancer cells were detected by qRT-PCR on blood for cytokeratin 14 (*Krt14*, not present in blood from healthy mice). Lung metastatic nodules were contrasted after intratracheal injection of 15% India ink solution. Macrophage depletion was achieved by daily i.p. injection of 20 mg/kg mouse anti-CSF-1R antibodies (clone AFS98; BioXcell) or isotype IgG control (Sigma-Aldrich). Mice were pretreated for 3 days with anti-CSF-1R before LLC tumor cell injection. Acute deletion of PFKFB3 was obtained by i.p. injection of tamoxifen (1 mg/mouse/day) for 5 days before subcutaneous implantation of LLC cancer cells. Torin2 was given by daily gavage at 20 mg/kg.

Hypoxia Assessment

Tumor hypoxia was detected 1 hr after i.p. injection of 60 mg/kg pimonidazole hydrochloride into tumor-bearing mice. Mice were sacrificed and tumors harvested. To detect the formation of pimonidazole adducts, tumor cryosections were immunostained with Hypoxyprobe-1-Mab1 (Hypoxyprobe kit; Chemicon) following the manufacturer's instructions.

(B and C) Percentage of continuous (quiescent) or discontinuous (remodeling) VE-cadherin junctions in HUVECs co-cultured on a 0.4-μm-pore Boyden chamber with hypoxic TAMs-L in the lower compartment in either 0.6 or 5.5 mM glucose (B) and representative images of VE-cadherin staining in the HUVEC monolayer (C).

(D) Transendothelial electrical resistance of a HUVEC monolayer co-cultured with hypoxic TAMs-L in either 0.6 or 5.5 mM glucose. Representative graphs of two independent experiments, total mice six per genotype in technical triplicates.

(E) Representative confocal images of CD31^{+} blood vessel morphology in tumors of WT mice transplanted with REDD1-deficient BM conditionally lacking *Pfkfb3* in macrophages only (REDD1$^{bm\Delta}$PFK$^{mo\Delta}$) or with the relative control BM cells.

(F and G) αSMA^{+} pericyte coverage.

(H and I) Lectin-FITC^{+} perfusion.

(J and K) Pimonidazole-positive hypoxic tumor area.

(L and M) LLC tumor growth (L) and weight at the time of dissection (M).

(N) Quantification of the number of lung metastases.

(O) In vivo 2NBDG glucose uptake in TAMs and tECs. Total mice six per condition.

(P) Schematic overview of the data showing that deletion of REDD1 triggers mTOR activity in hypoxic TAMs, which enhances glucose uptake and glycolysis. Highly glycolytic REDD1 KO TAMs enter in competition with tumor ECs for glucose, which leads to endothelial quiescence and vessel maturation, which prevents hypoxia and metastasis. In WT TAMs, massive REDD1 induction by hypoxia and other tumor-related stimuli brakes their glycolytic metabolism. As a result, glucose competition is not installed, while their release of angiogenic factors promotes the formation of abnormal and leaky blood vessels, overall favoring cancer cell intravasation and metastasis.

All experiments, total mice ten per genotype. *$p < 0.05$ versus WT or REDD1^{wt}; #$p < 0.05$ versus 0.6 mM glucose or PFK^{wt}. The scale bars represent 10 μm (C), 50 μm (E), and 100 μm (G, I, and K). All graphs show mean ± SEM. See also Figures S3 and S4 and Table S2.

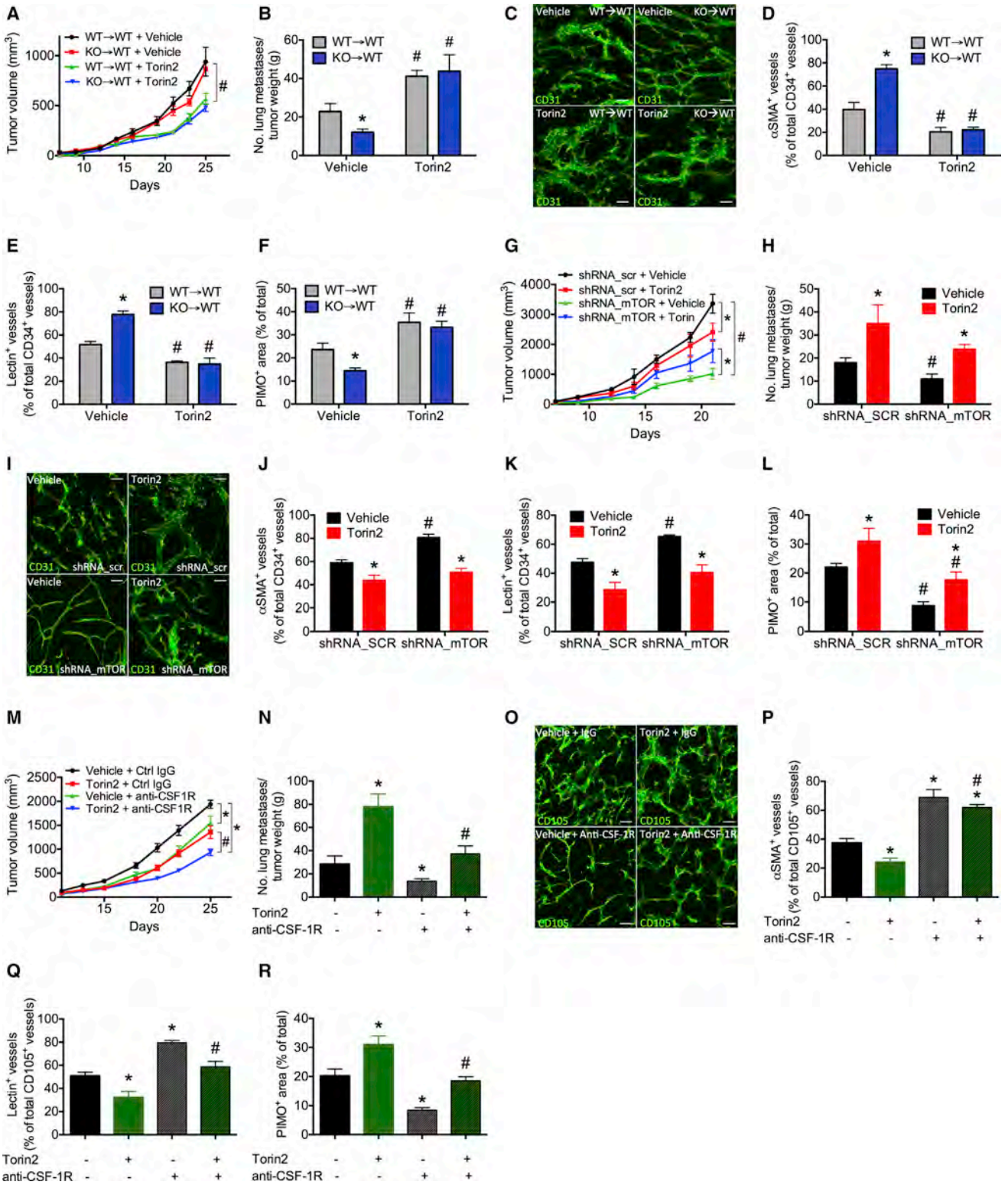

Figure 7. Opposing Activity of mTOR in Cancer Cells and TAMs

(A and B) LLC tumor growth (A) and metastatic index (B) in BM-transplanted mice treated with vehicle or Torin2.

(C–F) Representative images of CD31-stained thick sections (C), pericyte coverage (D), blood vessel perfusion (E), and hypoxia (F) in LLC tumors from mice treated with vehicle or Torin2. Total mice eight per condition.

(legend continued on next page)

Blood Vessel Perfusion and Leakiness

Perfused tumor vessels were counted on tumor sections from mice injected intravenously with 0.05 mg fluorescein isothiocyanate (FITC)-conjugated lectin (*Lycopersicon esculentum*; Vector Laboratories). Leaky blood vessels were histologically assessed upon intravenous injection of 70 kDa biotin-conjugated dextran (Molecular Probes). After 10 min, mice were perfused by intracardiac injection of saline for 5 min, and tumors were collection in 2% paraformaldehyde (PFA).

FACS of Tissue- and Tumor-Associated Macrophages

Tumor-bearing mice were sacrificed by cervical dislocation and tumors were harvested. Tumors or other organs were minced in RPMI medium containing 0.1% collagenase type I and 0.2% dispase type I and incubated in the same solution for 30 min at 37°C. The myeloid cell population in the tumor single cell suspension was enriched by magnetic isolation, using CD11b-conjugated magnetic beads, and subsequently stained for GLUT1 and the pan-macrophage marker F4/80.

Metabolic Assays

Glycolysis and oxidation of other substrates were determined on sorted GLUT1$^{low/-}$ and GLUT1^{high} CD11b^{+} F4/80^{+} TAMs directly or, when indicated, after overnight incubation with or without 100 nM Torin2 in normoxia or hypoxia, respectively, using radioactively labeled tracers. Oxygen consumption rate (OCR) was measured using the Seahorse XF24 analyzer. To characterize glucose uptake in vivo, LLC tumor-bearing mice were injected intratumorally with 2-NBDG, and F4/80^{+} TAMs and CD31^{+} ECs were analyzed using FACS.

Macrophage-EC Co-culture In Vitro

BMDMs (5×10^5) were seeded in a 24-well plate and differentiated to hypoxic TAMs-L (see above). The cells were then washed and incubated in M199 medium containing 5% fetal bovine serum and 0.6 or 5.5 mM glucose together with 5×10^4 HUVECs seeded 2 days before on a 0.4-μm-pore Boyden chamber insert (Corning). For VE-cadherin analysis, inserts containing the HUVEC monolayer were fixed after 8 hr of co-culture with 4% PFA for 7 min and stained with goat anti-VE-cadherin (R&D Systems). Transendothelial electrical resistance was measured with the EVOM2 Epithelial Voltohmeter (World Precision Instruments) after 24 hr of co-culture.

Statistical Analysis

Data entry and all analyses were performed in a blinded fashion. All statistical analyses were performed using GraphPad Prism software. Statistical significance was calculated using two-tailed unpaired t tests on two experimental conditions or two-way ANOVA when repeated measures were compared, with $p < 0.05$ considered statistically significant. All graphs show mean values ± SEM.

ACCESSION NUMBERS

The accession number for the RNA sequencing data reported in this paper is ArrayExpress: E-MTAB-5032.

SUPPLEMENTAL INFORMATION

Supplemental Information includes Supplemental Experimental Procedures, five figures, and two tables and can be found with this article online at http://dx.doi.org/10.1016/j.cmet.2016.09.008.

AUTHOR CONTRIBUTIONS

M.W. performed experimental design, all experiments, and data acquisition and interpretation, and wrote the manuscript. M.S. performed mouse treatments and dissections. M.D.M. contributed to the execution of clonings and qRT-PCR. R.M.-P. performed mouse treatments and FACS. J.S. and H.P. contributed to histological quantifications. J.G. analyzed RNA sequencing data. B.G. performed and analyzed liquid chromatography-mass spectrometry (LC-MS) experiments. P.C. provided the infrastructure and experimental design of metabolic experiments. M.M. performed experimental design and data analysis, conducted scientific direction, and wrote the manuscript.

ACKNOWLEDGMENTS

We thank Quark Pharmaceuticals for permission to use their proprietary REDD1 KO mice and Dr. Favier (University of Montpellier) for agreeing to supply these mice. The *Csf1r.Mer2.Cre* line was provided by Dr. Pollard (University of Edinburgh) and the *Pfkfb3*$^{lox/lox}$ by Dr. Chesney (University of Louisville). RNA sequencing was performed by VIB Nucleomics Core (http://www.nucleomics.be). M.M. was supported by a European Research Council (ERC) starting grant (OxyMO) (308459), Fonds Wetenschappelijk Onderzoek (FWO) (G066515N), Stichting tegen Kanker, and King Baudouin Foundation. R.M.-P. is funded by FWO. P.C. is supported by FWO, a federal government of Belgium grant (IUAP P7/03), and long-term structural Methusalem funding from the Flemish government.

Received: May 2, 2016
Revised: August 10, 2016
Accepted: September 21, 2016
Published: October 20, 2016

REFERENCES

Ahn, G.O., and Brown, J.M. (2008). Matrix metalloproteinase-9 is required for tumor vasculogenesis but not for angiogenesis: role of bone marrow-derived myelomonocytic cells. Cancer Cell *13*, 193–205.

Airley, R.E., Loncaster, J., Raleigh, J.A., Harris, A.L., Davidson, S.E., Hunter, R.D., West, C.M., and Stratford, I.J. (2003). GLUT-1 and CAIX as intrinsic markers of hypoxia in carcinoma of the cervix: relationship to pimonidazole binding. Int. J. Cancer *104*, 85–91.

Allen, E., Miéville, P., Warren, C.M., Saghafinia, S., Li, L., Peng, M.W., and Hanahan, D. (2016). Metabolic symbiosis enables adaptive resistance to anti-angiogenic therapy that is dependent on mTOR signaling. Cell Rep. *15*, 1144–1160.

Bentley, K., Franco, C.A., Philippides, A., Blanco, R., Dierkes, M., Gebala, V., Stanchi, F., Jones, M., Aspalter, I.M., Cagna, G., et al. (2014). The role of differential VE-cadherin dynamics in cell rearrangement during angiogenesis. Nat. Cell Biol. *16*, 309–321.

Brugarolas, J., Lei, K., Hurley, R.L., Manning, B.D., Reiling, J.H., Hafen, E., Witters, L.A., Ellisen, L.W., and Kaelin, W.G., Jr. (2004). Regulation of mTOR function in response to hypoxia by REDD1 and the TSC1/TSC2 tumor suppressor complex. Genes Dev. *18*, 2893–2904.

Byles, V., Covarrubias, A.J., Ben-Sahra, I., Lamming, D.W., Sabatini, D.M., Manning, B.D., and Horng, T. (2013). The TSC-mTOR pathway regulates macrophage polarization. Nat. Commun. *4*, 2834.

(G and H) Tumor growth (G) and metastatic index (H) in mice injected with LLC cells constitutively silenced (shRNA_mTOR) or not (shRNA_scr) for mTOR and treated with vehicle or Torin2. shRNA, short hairpin RNA.
(I–L) Representative images of CD31-stained thick sections (I), pericyte coverage (J), blood vessel perfusion (K), and tumor hypoxia (L). Total mice six to eight per condition.
(M and N) LLC tumor growth (M) and metastatic index (N) in mice treated with vehicle or Torin2, in combination with IgG or anti-CSF-1R.
(O–R) Representative images of CD31-stained thick sections (O), pericyte coverage (P), blood vessel perfusion (Q), and hypoxia (R). Total mice eight per condition.
*$p < 0.05$ versus WT → WT (A–F), vehicle (G–L), or vehicle and IgG (M–R); #$p < 0.05$ versus vehicle (A–F), shRNA_SCR (G–L), or Torin2 single treatment (M–R). The scale bars represent 50 μm. All graphs show mean ± SEM.

Casazza, A., Laoui, D., Wenes, M., Rizzolio, S., Bassani, N., Mambretti, M., Deschoemaeker, S., Van Ginderachter, J.A., Tamagnone, L., and Mazzone, M. (2013). Impeding macrophage entry into hypoxic tumor areas by Sema3A/Nrp1 signaling blockade inhibits angiogenesis and restores antitumor immunity. Cancer Cell *24*, 695–709.

Chen, Q., Zhang, X.H., and Massagué, J. (2011). Macrophage binding to receptor VCAM-1 transmits survival signals in breast cancer cells that invade the lungs. Cancer Cell *20*, 538–549.

Chesney, J., Telang, S., Yalcin, A., Clem, A., Wallis, N., and Bucala, R. (2005). Targeted disruption of inducible 6-phosphofructo-2-kinase results in embryonic lethality. Biochem. Biophys. Res. Commun. *331*, 139–146.

Cloughesy, T.F., Yoshimoto, K., Nghiemphu, P., Brown, K., Dang, J., Zhu, S., Hsueh, T., Chen, Y., Wang, W., Youngkin, D., et al. (2008). Antitumor activity of rapamycin in a Phase I trial for patients with recurrent PTEN-deficient glioblastoma. PLoS Med. *5*, e8.

Colegio, O.R., Chu, N.Q., Szabo, A.L., Chu, T., Rhebergen, A.M., Jairam, V., Cyrus, N., Brokowski, C.E., Eisenbarth, S.C., Phillips, G.M., et al. (2014). Functional polarization of tumour-associated macrophages by tumour-derived lactic acid. Nature *513*, 559–563.

De Bock, K., Georgiadou, M., Schoors, S., Kuchnio, A., Wong, B.W., Cantelmo, A.R., Quaegebeur, A., Ghesquière, B., Cauwenberghs, S., Eelen, G., et al. (2013). Role of PFKFB3-driven glycolysis in vessel sprouting. Cell *154*, 651–663.

Don, A.S., and Zheng, X.F. (2011). Recent clinical trials of mTOR-targeted cancer therapies. Rev. Recent Clin. Trials *6*, 24–35.

Ellisen, L.W., Ramsayer, K.D., Johannessen, C.M., Yang, A., Beppu, H., Minda, K., Oliner, J.D., McKeon, F., and Haber, D.A. (2002). REDD1, a developmentally regulated transcriptional target of p63 and p53, links p63 to regulation of reactive oxygen species. Mol. Cell *10*, 995–1005.

Fantin, A., Vieira, J.M., Gestri, G., Denti, L., Schwarz, Q., Prykhozhij, S., Peri, F., Wilson, S.W., and Ruhrberg, C. (2010). Tissue macrophages act as cellular chaperones for vascular anastomosis downstream of VEGF-mediated endothelial tip cell induction. Blood *116*, 829–840.

Finisguerra, V., Di Conza, G., Di Matteo, M., Serneels, J., Costa, S., Thompson, A.A., Wauters, E., Walmsley, S., Prenen, H., Granot, Z., et al. (2015). MET is required for the recruitment of anti-tumoural neutrophils. Nature *522*, 349–353.

Freemerman, A.J., Johnson, A.R., Sacks, G.N., Milner, J.J., Kirk, E.L., Troester, M.A., Macintyre, A.N., Goraksha-Hicks, P., Rathmell, J.C., and Makowski, L. (2014). Metabolic reprogramming of macrophages: glucose transporter 1 (GLUT1)-mediated glucose metabolism drives a proinflammatory phenotype. J. Biol. Chem. *289*, 7884–7896.

Gatenby, R.A., and Gillies, R.J. (2004). Why do cancers have high aerobic glycolysis? Nat. Rev. Cancer *4*, 891–899.

Guba, M., von Breitenbuch, P., Steinbauer, M., Koehl, G., Flegel, S., Hornung, M., Bruns, C.J., Zuelke, C., Farkas, S., Anthuber, M., et al. (2002). Rapamycin inhibits primary and metastatic tumor growth by antiangiogenesis: involvement of vascular endothelial growth factor. Nat. Med. *8*, 128–135.

Han, R., Gao, J., Zhai, H., Xiao, J., Ding, Y., and Hao, J. (2016). RAD001 (everolimus) attenuates experimental autoimmune neuritis by inhibiting the mTOR pathway, elevating Akt activity and polarizing M2 macrophages. Exp. Neurol. *280*, 106–114.

Henze, A.T., and Mazzone, M. (2016). The impact of hypoxia on tumor-associated macrophages. J. Clin. Invest., Published online August 2, 2016. http://dx.doi.org/10.1172/JCI84427.

Ho, P.C., Bihuniak, J.D., Macintyre, A.N., Staron, M., Liu, X., Amezquita, R., Tsui, Y.C., Cui, G., Micevic, G., Perales, J.C., et al. (2015). Phosphoenolpyruvate is a metabolic checkpoint of anti-tumor T cell responses. Cell *162*, 1217–1228.

Horak, P., Crawford, A.R., Vadysirisack, D.D., Nash, Z.M., DeYoung, M.P., Sgroi, D., and Ellisen, L.W. (2010). Negative feedback control of HIF-1 through REDD1-regulated ROS suppresses tumorigenesis. Proc. Natl. Acad. Sci. U S A *107*, 4675–4680.

Hsieh, A.C., Liu, Y., Edlind, M.P., Ingolia, N.T., Janes, M.R., Sher, A., Shi, E.Y., Stumpf, C.R., Christensen, C., Bonham, M.J., et al. (2012). The translational landscape of mTOR signalling steers cancer initiation and metastasis. Nature *485*, 55–61.

Laoui, D., Van Overmeire, E., Di Conza, G., Aldeni, C., Keirsse, J., Morias, Y., Movahedi, K., Houbracken, I., Schouppe, E., Elkrim, Y., et al. (2014). Tumor hypoxia does not drive differentiation of tumor-associated macrophages but rather fine-tunes the M2-like macrophage population. Cancer Res. *74*, 24–30.

Laplante, M., and Sabatini, D.M. (2012). mTOR signaling in growth control and disease. Cell *149*, 274–293.

Li, J., Kim, S.G., and Blenis, J. (2014). Rapamycin: one drug, many effects. Cell Metab. *19*, 373–379.

Lin, L., Stringfield, T.M., Shi, X., and Chen, Y. (2005). Arsenite induces a cell stress-response gene, RTP801, through reactive oxygen species and transcription factors Elk-1 and CCAAT/enhancer-binding protein. Biochem. J. *392*, 93–102.

Maes, H., Kuchnio, A., Peric, A., Moens, S., Nys, K., De Bock, K., Quaegebeur, A., Schoors, S., Georgiadou, M., Wouters, J., et al. (2014). Tumor vessel normalization by chloroquine independent of autophagy. Cancer Cell *26*, 190–206.

Mantovani, A., and Allavena, P. (2015). The interaction of anticancer therapies with tumor-associated macrophages. J. Exp. Med. *212*, 435–445.

Mantovani, A., Sozzani, S., Locati, M., Allavena, P., and Sica, A. (2002). Macrophage polarization: tumor-associated macrophages as a paradigm for polarized M2 mononuclear phagocytes. Trends Immunol. *23*, 549–555.

Mazzieri, R., Pucci, F., Moi, D., Zonari, E., Ranghetti, A., Berti, A., Politi, L.S., Gentner, B., Brown, J.L., Naldini, L., and De Palma, M. (2011). Targeting the ANG2/TIE2 axis inhibits tumor growth and metastasis by impairing angiogenesis and disabling rebounds of proangiogenic myeloid cells. Cancer Cell *19*, 512–526.

Mazzone, M., Dettori, D., Leite de Oliveira, R., Loges, S., Schmidt, T., Jonckx, B., Tian, Y.M., Lanahan, A.A., Pollard, P., Ruiz de Almodovar, C., et al. (2009). Heterozygous deficiency of PHD2 restores tumor oxygenation and inhibits metastasis via endothelial normalization. Cell *136*, 839–851.

Mosser, D.M., and Edwards, J.P. (2008). Exploring the full spectrum of macrophage activation. Nat. Rev. Immunol. *8*, 958–969.

Murdoch, C., Muthana, M., Coffelt, S.B., and Lewis, C.E. (2008). The role of myeloid cells in the promotion of tumour angiogenesis. Nat. Rev. Cancer *8*, 618–631.

Qian, B.Z., Li, J., Zhang, H., Kitamura, T., Zhang, J., Campion, L.R., Kaiser, E.A., Snyder, L.A., and Pollard, J.W. (2011). CCL2 recruits inflammatory monocytes to facilitate breast-tumour metastasis. Nature *475*, 222–225.

Rademakers, S.E., Lok, J., van der Kogel, A.J., Bussink, J., and Kaanders, J.H. (2011). Metabolic markers in relation to hypoxia; staining patterns and colocalization of pimonidazole, HIF-1α, CAIX, LDH-5, GLUT-1, MCT1 and MCT4. BMC Cancer *11*, 167.

Rodríguez-Prados, J.C., Través, P.G., Cuenca, J., Rico, D., Aragonés, J., Martín-Sanz, P., Cascante, M., and Boscá, L. (2010). Substrate fate in activated macrophages: a comparison between innate, classic, and alternative activation. J. Immunol. *185*, 605–614.

Rolny, C., Mazzone, M., Tugues, S., Laoui, D., Johansson, I., Coulon, C., Squadrito, M.L., Segura, I., Li, X., Knevels, E., et al. (2011). HRG inhibits tumor growth and metastasis by inducing macrophage polarization and vessel normalization through downregulation of PlGF. Cancer Cell *19*, 31–44.

Sennino, B., Ishiguro-Oonuma, T., Wei, Y., Naylor, R.M., Williamson, C.W., Bhagwandin, V., Tabruyn, S.P., You, W.K., Chapman, H.A., Christensen, J.G., et al. (2012). Suppression of tumor invasion and metastasis by concurrent inhibition of c-Met and VEGF signaling in pancreatic neuroendocrine tumors. Cancer Discov. *2*, 270–287.

Shigeoka, M., Urakawa, N., Nakamura, T., Nishio, M., Watajima, T., Kuroda, D., Komori, T., Kakeji, Y., Semba, S., and Yokozaki, H. (2013). Tumor associated macrophage expressing CD204 is associated with tumor aggressiveness of esophageal squamous cell carcinoma. Cancer Sci. *104*, 1112–1119.

Sica, A., and Mantovani, A. (2012). Macrophage plasticity and polarization: in vivo veritas. J. Clin. Invest. *122*, 787–795.

Song, S., Abdelmohsen, K., Zhang, Y., Becker, K.G., Gorospe, M., and Bernier, M. (2011). Impact of pyrrolidine dithiocarbamate and interleukin-6 on mammalian target of rapamycin complex 1 regulation and global protein translation. J. Pharmacol. Exp. Ther. *339*, 905–913.

Stefater, J.A., 3rd, Lewkowich, I., Rao, S., Mariggi, G., Carpenter, A.C., Burr, A.R., Fan, J., Ajima, R., Molkentin, J.D., Williams, B.O., et al. (2011). Regulation of angiogenesis by a non-canonical Wnt-Flt1 pathway in myeloid cells. Nature *474*, 511–515.

Sun, S., Chen, S., Liu, F., Wu, H., McHugh, J., Bergin, I.L., Gupta, A., Adams, D., and Guan, J.L. (2015). Constitutive activation of mTORC1 in endothelial cells leads to the development and progression of lymphangiosarcoma through VEGF autocrine signaling. Cancer Cell *28*, 758–772.

Taha, C., Liu, Z., Jin, J., Al-Hasani, H., Sonenberg, N., and Klip, A. (1999). Opposite translational control of GLUT1 and GLUT4 glucose transporter mRNAs in response to insulin. Role of mammalian target of rapamycin, protein kinase b, and phosphatidylinositol 3-kinase in GLUT1 mRNA translation. J. Biol. Chem. *274*, 33085–33091.

Takeuchi, H., Tanaka, M., Tanaka, A., Tsunemi, A., and Yamamoto, H. (2016). Predominance of M2-polarized macrophages in bladder cancer affects angiogenesis, tumor grade and invasiveness. Oncol. Lett. *11*, 3403–3408.

Tannahill, G.M., Curtis, A.M., Adamik, J., Palsson-McDermott, E.M., McGettrick, A.F., Goel, G., Frezza, C., Bernard, N.J., Kelly, B., Foley, N.H., et al. (2013). Succinate is an inflammatory signal that induces IL-1β through HIF-1α. Nature *496*, 238–242.

Vats, D., Mukundan, L., Odegaard, J.I., Zhang, L., Smith, K.L., Morel, C.R., Wagner, R.A., Greaves, D.R., Murray, P.J., and Chawla, A. (2006). Oxidative metabolism and PGC-1beta attenuate macrophage-mediated inflammation. Cell Metab. *4*, 13–24.

Wang, Z., Malone, M.H., Thomenius, M.J., Zhong, F., Xu, F., and Distelhorst, C.W. (2003). Dexamethasone-induced gene 2 (dig2) is a novel pro-survival stress gene induced rapidly by diverse apoptotic signals. J. Biol. Chem. *278*, 27053–27058.

Xian, X., Håkansson, J., Ståhlberg, A., Lindblom, P., Betsholtz, C., Gerhardt, H., and Semb, H. (2006). Pericytes limit tumor cell metastasis. J. Clin. Invest. *116*, 642–651.

Zhu, L., Yang, T., Li, L., Sun, L., Hou, Y., Hu, X., Zhang, L., Tian, H., Zhao, Q., Peng, J., et al. (2014). TSC1 controls macrophage polarization to prevent inflammatory disease. Nat. Commun. *5*, 4696.